Kinetic Energy Release in Thermal Ion–Molecule Reactions: Single Charge-Transfer Reactions of V^{2+} and Ta^{2+} with Benzene

James R. Gord,† Ben S. Freiser,*

Herbert C. Brown Laboratory of Chemistry, Purdue University, West Lafayette, Indiana 47907

and Steven W. Buckner

Department of Chemistry, University of Arizona, Tucson, Arizona 85721 *(Received: May 30, 1990; In Final Form: January 22, 1991)*

Fourier transform ion cyclotron resonance mass spectrometry (FTICRMS) has been used to study the single charge-transfer reactions of V^{2+} and Ta^{2+} with benzene under thermal conditions. Thermal charge-transfer rate constants of 2.0×10^{-9} and 1.2×10^{-9} cm^3 molecule^{-1} s^{-1} were measured for V^{2+} and Ta^{2+}, respectively. The total kinetic energy of the product ions was determined to be 1.91 ± 0.50 eV for the V^{2+} case and 2.82 ± 0.50 eV for the Ta^{2+} case. These results and a previous study of the Nb^{2+}–benzene single charge-transfer system suggest a simple long-distance electron-transfer mechanism proceeding by ionization of the $1a_{2u}$ orbital of benzene with significant internal excitation of the nascent $C_6H_6^+$ product.

Introduction

A number of recent studies of transition-metal dications have demonstrated that these species have fascinating properties.[1-5] These investigations have focused on the mechanistic, kinetic, and dynamic aspects of the reactions of doubly charged transition-metal ions with small hydrocarbons in the gas phase. In particular, doubly charged metal–ligand species generated through the reaction of Nb^{2+} with small alkanes have been shown to be thermodynamically stable with significant metal–ligand bond energies.[4] Many of the results of these studies can be rationalized in terms of a simple Landau–Zener curve-crossing model.

We recently studied the reaction kinetics and energy disposal in the single charge-transfer reaction between Nb^{2+} and benzene.[5] Given the exothermicity of the reaction, 5.08 eV, our measurements of the kinetic energies of Nb^+, 0.81 ± 0.25 eV, and $C_6H_6^+$, 1.22 ± 0.25 eV, indicate that 3.05 ± 0.50 eV is partitioned to the internal modes of the product ions. In addition, the kinetic energy release measurements were well fit by a single-valued energy for each product ion, suggesting that the reaction proceeds to produce a narrow distribution of product kinetic and internal energies. These data and the high efficiency of the reaction indicated by the kinetics studies were rationalized in terms of a long-distance electron-transfer mechanism producing electronically excited $C_6H_6^+$ through ionization of the $1a_{2u}$ orbital of benzene, which lies $\sim$3 eV above the ground state of the benzene cation.[6]

In this study we have extended our original experiments to include the single charge-transfer reactions of two other group 5 transition-metal dications, V^{2+} and Ta^{2+}, with benzene. The reaction kinetics and kinetic energy releases observed in these two cases provide further support for the long-distance electron-transfer mechanism while raising questions concerning the simple energy partitioning model. The narrow kinetic energy distributions indicated in this study are consistent with a reaction mechanism proceeding to produce electronically excited $C_6H_6^+$; however, the internal energies deposited in the products suggest that more complex dynamics may be involved and that both the metal ion product and $C_6H_6^+$ may be electronically excited.

Experimental Section

Reaction kinetics were studied by using a Nicolet FTMS-2000 Fourier transform ion cyclotron resonance mass spectrometer[7] equipped with a rectangular trapping cell (4.76 cm × 4.76 cm × 9.52 cm) in a 3-T magnetic field. Singly and doubly charged metal ions were generated by focusing the fundamental output (1064 nm) of a Q-switched Nd:YAG laser onto any of various pure metal targets maintained in an external ion source.[8,9] In an effort to cool kinetically and internally excited laser-desorbed ions,[10] they were trapped for 500 ms with 3.3×10^{-8} Torr of benzene (Baker, spectral grade) and 2×10^{-6} Torr of argon (Airco) introduced by using Varian-controlled leak valves. Pressure measurement was achieved with a Bayard-Alpert ionization gauge calibrated by using acetone in reaction 1, which

$$C_3H_6O^+ + C_3H_6O \rightarrow \text{products} \qquad (1)$$

proceeds with a rate constant of 5.4×10^{-10} cm^3 molecule^{-1} s^{-1},[11] and corrected for ion gauge sensitivity by using the R_x factors of Bartmess and Georgiadis.[12] Swept double-resonance pulses[13] were used to isolate M^{2+} after thermalization. Kinetics experiments were performed at trapping voltages of 5 V to ensure that all kinetically excited product ions were efficiently trapped.

Kinetic energy releases were measured by using a previously described technique.[5,14-31] Briefly, ion kinetic energies can be

† National Science Foundation predoctoral fellow, ACS Analytical Division fellow. Present address: Joint Institute for Laboratory Astrophysics, University of Colorado and National Institute of Standards and Technology, Boulder, CO 80309.

* To whom correspondence should be addressed.

(1) Tonkyn, R.; Weisshaar, J. C. *J. Am. Chem. Soc.* **1986**, *108*, 7128.
(2) Buckner, S. W.; Freiser, B. S. *J. Am. Chem. Soc.* **1987**, *109*, 1247.
(3) Huang, Y.; Freiser, B. S. *J. Am. Chem. Soc.* **1988**, *110*, 4435.
(4) Gord, J. R.; Freiser, B. S.; Buckner, S. W. *J. Chem. Phys.* **1989**, *91*, 7530.
(5) Gord, J. R.; Freiser, B. S.; Buckner, S. W. *J. Chem. Phys.* **1991**, *94*, 4282.
(6) Kimura, K.; Katsumata, S.; Achiba, Y.; Yamazaki, T.; Iwata, S. *Handbook of He(I) Photoelectron Spectra*; Japan Scientific Societies Press: Tokyo, 1981; p 188.
(7) For a recent review of FTICRMS methodologies applied in our laboratory see: Freiser, B. S. *Chemtracts* **1989**, *1*, 65.
(8) Cody, R. B.; Burnier, R. C.; Reents, Jr., W. D.; Carlin, T. J.; McCrery, D. A.; Lengel, R. K.; Freiser, B. S. *Int. J. Mass Spectrom. Ion Phys.* **1980**, *33*, 37.
(9) Weller, R. R.; Ghaderi, S.; Vorburger, O.; Freiser, B. S. *Proceedings of the 36th ASMS Conference on Mass Spectrometry and Allied Topics*; San Francisco, CA, June 5–10, 1988; pp 614–615.
(10) Kang, H.; Beauchamp, J. L. *J. Phys. Chem.* **1985**, *89*, 3364.
(11) MacNeil, K. A. G.; Futrell, J. H. *J. Phys. Chem.* **1972**, *76*, 409.
(12) Bartmess, J. E.; Georgiadis, R. M. *Vacuum* **1983**, *33*, 149.
(13) Comisarow, M. B.; Parisod, G.; Grassi, V. *Chem. Phys. Lett.* **1978**, *57*, 413.
(14) Dunbar, R. C.; Kramer, J. M. *J. Chem. Phys.* **1973**, *58*, 1266.
(15) Orth, R.; Dunbar, R. C.; Riggin, M. *Chem. Phys.* **1977**, *19*, 279.
(16) Marx, R.; Mauclaire, G.; Derai, R. *Int. J. Mass Spectrom. Ion Phys.* **1983**, *47*, 155.
(17) Derai, R.; Mauclaire, G.; Marx, R. *Chem. Phys. Lett.* **1982**, *86*, 275.
(18) Marx, R. In *Lecture Notes in Chemistry*; Hartmann, H., Wanczek, K. P., Eds.; Springer-Verlag: West Berlin, 1982; Vol. 31, p 272.
(19) Mauclaire, G.; Derai, R.; Fenistein, S.; Marx, R. *J. Chem. Phys.* **1979**, *70*, 4023.
(20) Marx, R. *NATO ASI Ser., Ser. B* **1979**, *B40*, 103.
(21) Derai, R.; Fenistein, S.; Gerard-Ain, M.; Grovers, T. R.; Marx, R.; Mauclair, G.; Profous, C. Z.; Sourisseau, C. *Chem. Phys.* **1979**, *44*, 65.
(22) Mauclaire, G.; Derai, R.; Fenistein, S.; Marx, R. *J. Chem. Phys.* **1979**, *70*, 4017.

0022-3654/91/2095-8274$02.50/0

determined on the basis of the voltage dependence of the fraction of the ions trapped. When the electrostatic trapping well employed in the ICR is sufficiently deep, all of the ions will be trapped; however, as the well depth is decreased, kinetically excited ions will escape the trap. Plots of the fraction of the ions trapped, f, versus the square root of the trapping potential, $V_{trap}^{1/2}$, are expected to show two distinct linear regions described by

$$V_{trap} > E_k: \qquad f = 1$$

$$V_{trap} < E_k: \qquad f = (V_{trap}/E_k)^{1/2}$$

where E_k is the kinetic energy of the ions. The break between these two linear regions defines the kinetic energy of the ions.

These measurements were performed by using a Nicolet FTMS-2000 mass spectrometry data station interfaced to a single-cell ICR spectrometer equipped with a Varian 15-in. electromagnet operated at 0.85 T. The cell is cubic and measures 5.2 cm on a side. During the course of the experiments, benzene and argon were maintained at $\sim 5 \times 10^{-6}$ and $\sim 1 \times 10^{-4}$ Torr, respectively, as measured with an uncalibrated Bayard-Alpert ionization gauge.

The experimental pulse sequence was initiated with a quench pulse, followed by a laser shot to generate ions, and a 150-ms thermalization period during which the trapping voltage was dropped to 0.5 V to assist in the removal of kinetically excited ions. After thermalization and isolation of M^{2+}, the dication was permitted to react for 300 ms with benzene, and the ionic products of the reaction were detected under broadband excitation and digitization conditions. The trapping voltage was maintained at 8 V throughout each phase of the experiment, except during the quench, cooling, and reaction periods.

For each metal, four series of 66 experiments were performed in which the trapping voltage during the reaction period was varied from 0.5 to 7.0 V in steps of 0.1 V. At each voltage, 10 transients were averaged to obtain a mass spectrum. To account for shot-to-shot variations in the ion yield of the laser ionization source and to correct for voltage-dependent changes in the ion intensities not associated with the kinetic energy of the ions, the absolute intensities of the singly charged product ions, M^+ (M = V, Ta) and $C_6H_6^+$, were ratioed to the intensity of the thermalized doubly charged reactant ion, M^{2+}. This process ensures that changes in the relative abundances of the singly charged product ions with trapping voltage will reflect the kinetic energy of the ions.

Results

The reactions of V^{2+} and Ta^{2+} with benzene are dominated by single charge transfer. Reaction 2 is the only process observed

$$V^{2+} + C_6H_6 \rightarrow V^+ + C_6H_6^+ \qquad (2)$$

for V^{2+} with benzene. Reaction 3 accounts for the vast majority

$$Ta^{2+} + C_6H_6 \rightarrow Ta^+ + C_6H_6^+ \qquad (3)$$

of the products observed for Ta^{2+} with benzene; however, small signals ($\leq 5\%$) corresponding to the formation of Ta^{2+}(benzyne) and other bond-insertion products were also noted. Similar behavior was reported for Nb^{2+},[5] which reacts with benzene through charge transfer (95%) and dehydrogenation to generate Nb^{2+}-(benzyne) (5%).

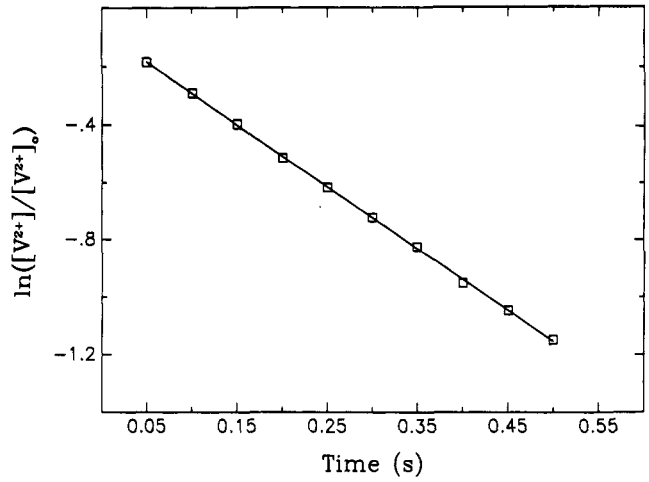

Figure 1. Pseudo-first-order kinetics plot for the decay of the V^{2+} signal during the reaction of V^{2+} with benzene.

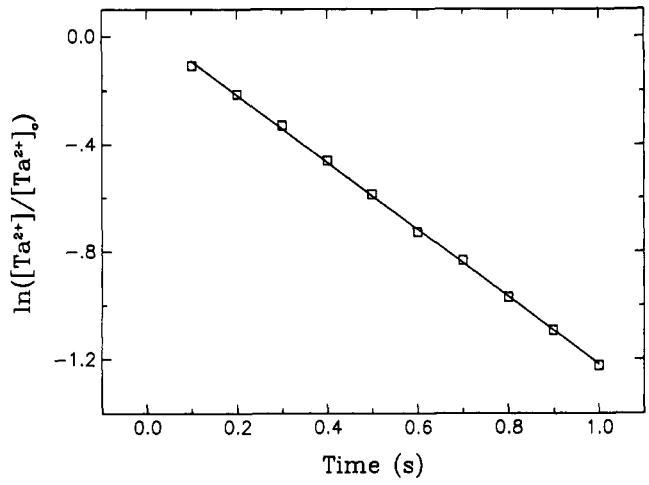

Figure 2. Pseudo-first-order kinetics plot for the decay of the Ta^{2+} signal during the reaction of Ta^{2+} with benzene.

The pseudo-first-order kinetics plots for the decay of M^{2+} with reaction time are depicted in Figures 1 and 2. On the basis of the calibrated benzene pressure, these plots indicate rate constants of 2.0×10^{-9} and 1.2×10^{-9} cm^3 molecule^{-1} s^{-1} for V^{2+} and Ta^{2+} with benzene, respectively. The Langevin rates for these systems are 2.72×10^{-9} and 2.05×10^{-9} cm^3 molecule^{-1} s^{-1}, from which reaction efficiencies, k/k_L, of 0.74 for V^{2+} and 0.59 for Ta^{2+} are determined. The absolute error in the rate constants is probably no more than ±30%. The linearity of these kinetics plots suggests that the metal dications are thermalized.

Kinetic energies released to the singly charged product ions in each case were determined from the f vs $V_{eff}^{1/2}$ plots prepared from the series of voltage-resolved mass spectra. Data analysis and the calculation of $V_{eff}^{1/2}$ have been described in detail previously.[5] Briefly, the raw intensity ratios, M^+/M^{2+} and $C_6H_6^+/M^{2+}$, were normalized and averaged (using the variance of the data in the $f = 1$ linear region as a weighting factor) to generate the kinetic energy plots. These were corrected for a small positive slope in the $f = 1$ region and a nonzero x intercept.[5,31] The origin of the positive slope in the $f = 1$ portion of the plot is still uncertain, but it appears to be associated with voltage-dependent effects of space charge on the spatial extent of the singly and doubly charged ion clouds. The nonzero x intercept arises through surface charging of the trapping plates, changing the effective well depth the ions experience. The corrected plots for V^+ and $C_6H_6^+$ produced in reaction 2 and Ta^+ and $C_6H_6^+$ produced in reaction 3 are displayed in Figures 3–6, respectively.

The solid lines through the experimental data represent a single-valued kinetic energy in each case convoluted with the shape

(23) Mauclaire, G.; Derai, R.; Marx, R. In *Dynamic Mass Spectrometry*; Price, D., Todd, J. F. J., Eds.; Heyden: London, 1978, Vol. 5, p 139.
(24) Rincon, M. E.; Pearson, J.; Bowers, M. T. *J. Phys. Chem.* **1988**, *92*, 4290.
(25) Rincon, M.; Pearson, J.; Bowers, M. T. *Int. J. Mass Spectrom. Ion Proc.* **1987**, *80*, 133.
(26) Bowers, M. T.; Rincon, M. *Faraday Discuss. Chem. Soc.* **1987**, *84*, 303.
(27) O'Keefe, A.; Mauclaire, G.; Parent, D.; Bowers, M. T. *J. Chem. Phys.* **1986**, *84*, 215.
(28) Parent, D. C.; Derai, R.; Mauclaire, G.; Heninger, M.; Marx, R.; Rincon, M. E.; O'Keefe, A.; Bowers, M. T. *Chem. Phys. Lett.* **1985**, *117*, 127.
(29) O'Keefe, A.; Parent, D.; Mauclaire, G.; Bowers, M. T. *J. Chem. Phys.* **1984**, *80*, 4901.
(30) Kemper, P. R.; Bowers, M. T.; Parent, D. C.; Mauclaire, G.; Derai, R.; Marx, R. *J. Chem. Phys.* **1983**, *79*, 160.
(31) Parent, D. Ph.D. Thesis, University of California Santa Barbara, 1983.

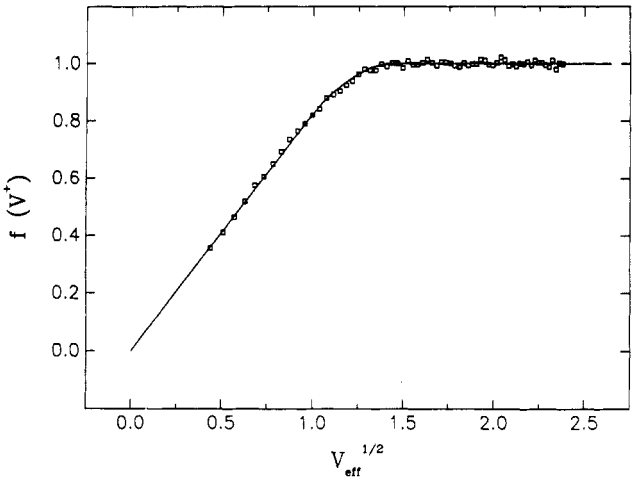

Figure 3. Kinetic energy plot for V^+ generated during the reaction of V^{2+} with benzene. The solid line represents a single-valued kinetic energy (0.99 eV) convoluted with the shape of the trapping well and fit to the experimental data.

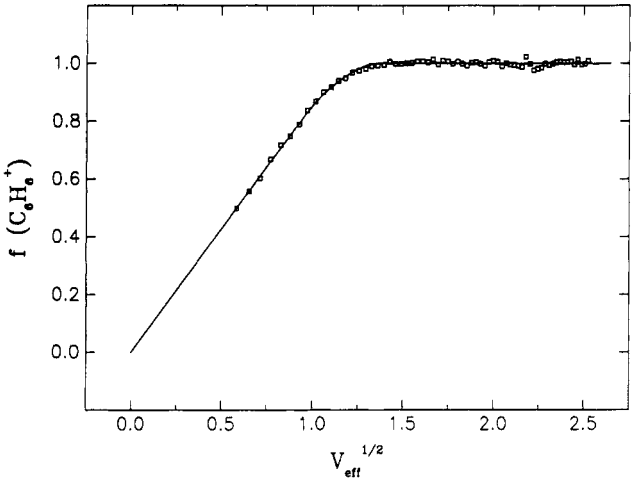

Figure 4. Kinetic energy plot for $C_6H_6^+$ generated during the reaction of V^{2+} with benzene. The solid line represents a single-valued kinetic energy (0.92 eV) convoluted with the shape of the trapping well and fit to the experimental data.

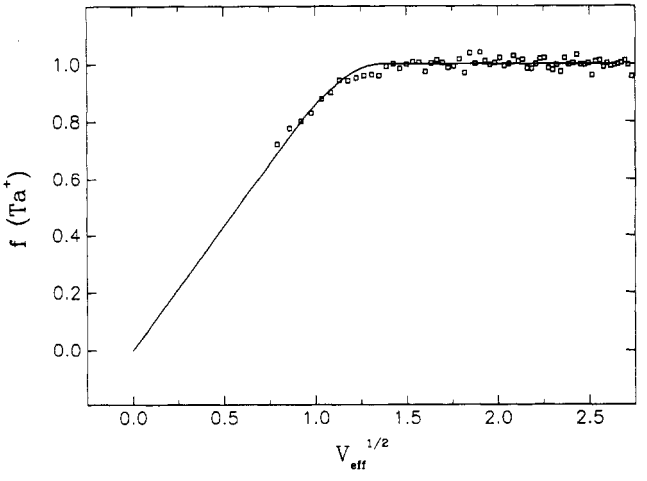

Figure 5. Kinetic energy plot for Ta^+ generated during the reaction of Ta^{2+} with benzene. The solid line represents a single-valued kinetic energy (0.90 eV) convoluted with the shape of the trapping well and fit to the experimental data.

of the electrostatic potential well and fit to the data by using least-squares methods. If all of the ions feel the same trapping potential, the break between the two linear regions is expected to be sharp. However, the spatial distribution of the ions in our experiment and the quadrupolar shape of the electrostatic trapping well in our cubic cell produce the smooth break between the regions observed in the experimental data and well fit by the solid line.

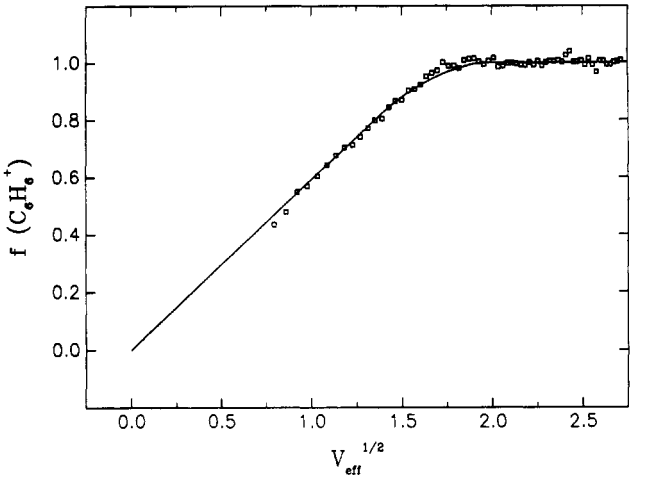

Figure 6. Kinetic energy plot for $C_6H_6^+$ generated during the reaction of Ta^{2+} with benzene. The solid line represents a single-valued kinetic energy (1.92 eV) convoluted with the shape of the trapping well and fit to the experimental data.

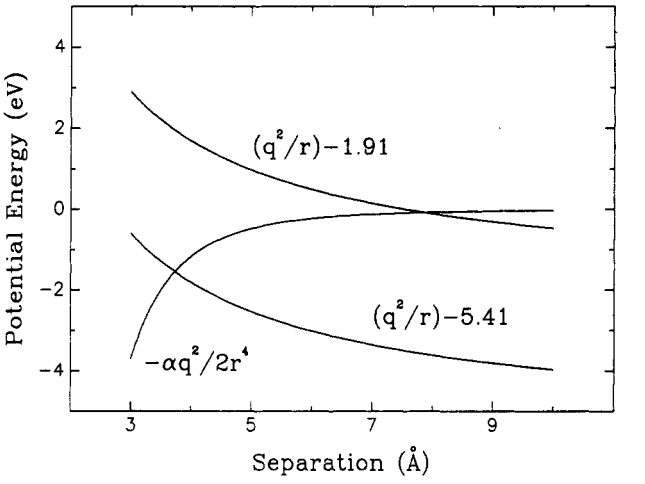

Figure 7. Potential energy curves for the V^{2+}–benzene charge-transfer reaction. Long-distance electron transfer occurs at ~7.9 Å. The ground-state curves, which cross at ~3.8 Å, are included for comparison.

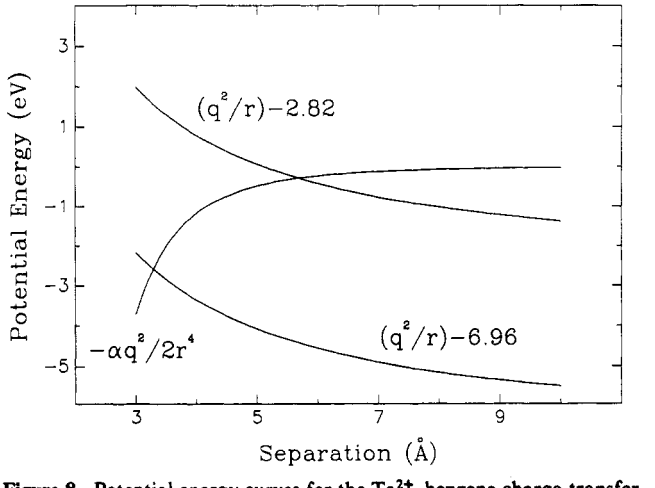

Figure 8. Potential energy curves for the Ta^{2+}–benzene charge-transfer reaction. Long-distance electron transfer occurs at ~5.7 Å. The ground-state curves, which cross at ~3.3 Å, are included for comparison.

The ion kinetic energies determined from the fits in the V^{2+} case are 0.99 ± 0.25 eV for V^+ and 0.92 ± 0.25 eV for $C_6H_6^+$, yielding a total kinetic energy deposited in the products of 1.91 ± 0.50 eV. In the Ta^{2+} case, the ion kinetic energies are 0.90 ± 0.25 eV for Ta^+ and 1.92 ± 0.25 eV for $C_6H_6^+$, for a total

TABLE I: Summary of Reaction Kinetics, Energy Partitioning, and Curve-Crossing Results for the Thermal Single Charge-Transfer Reactions of M^{2+} (M = V, Nb, Ta) with Benzene

	V	Nb	Ta
reaction rate k, $\times 10^9$ cm^3 molecule^{-1} s^{-1}	2.0	1.4	1.2
Langevin rate k_L, $\times 10^9$ cm^3 molecule^{-1} s^{-1}	2.72	2.32	2.05
reaction efficiency, k/k_L	0.74	0.60	0.59
2nd ionization potential, eV	14.65	14.32	16.2
charge-transfer exothermicity, eV	5.41	5.08	6.96
kinetic energy M^+,[a] eV	0.99	0.81	0.90
kinetic energy $C_6H_6^+$,[a] eV	0.92	1.22	1.92
total product kinetic energy,[b] eV	1.91	2.03	2.82
total product internal energy,[b] eV	3.50	3.05	4.14
calcd curve crossing, Å	7.9	7.5	5.7

[a] Experimental uncertainty in these values is ±0.25 eV. [b] Experimental uncertainty in these values is ±0.50 eV.

kinetic energy of 2.82 ± 0.50 eV.

On the basis of the measured kinetic energies, the reaction exothermicity partitioned to internal modes in each case can be determined by using

$$IE(M^+,C_6H_6^+) = IP(M^+) - IP(C_6H_6) - KE(M^+,C_6H_6^+)$$

The ionization potential of benzene is 9.24 eV,[32] while the second ionization potentials of V and Ta are 14.65 and 16.2 eV, respectively.[33] Therefore, the internal energy is 3.50 ± 0.50 eV in the V^{2+} reaction and 4.14 ± 0.50 eV in the Ta^{2+} reaction. All of these results, as well as the results for Nb^{2+} with benzene from ref 5, are summarized in Table I.

A number of factors contribute to the uncertainty in the kinetic energy release measurements, and these warrant further discussion. In addition to simple statistical fluctuations in the measured ion intensity ratios, two potentially major systematic errors contribute to the uncertainty of the experiment.

The first of these is associated with the shape of the electrostatic potential well (vide supra).[5,34,35] Since this well is approximately quadrupolar in shape, the potential experienced by a particular ion depends strongly on its location in the trapping cell. Assigning the direction of the magnetic field as the z axis, we fit the kinetic energy release plots assuming an ion population that is relaxed to the center of the cell along the z axis and in which ions are uniformly distributed in the xy plane at this position. The limitations of this spatial distribution model and our lack of information concerning the time evolution of the distribution of ions in the cell represent one source of systematic error.

A second and potentially more significant source lies in the nonzero x intercept correction described above. Since the kinetic energy of the ions is determined from a plot that scales with the square root of the effective trapping voltage, even small uncertainties in the depth of the trapping well can produce significant errors in the kinetic energy values. In light of these potential errors, we have assigned rather large error limits.

Finally, the kinetic energy plot for the Ta^+ product deserves special attention. Our procedure for correcting the nonzero x intercept involves fitting the linearly increasing portion of the kinetic energy plot via least-squares methods to find the value of the x intercept and subsequently substracting the calculated value of this intercept from all of the data. Typically, this intercept value is nearly zero or slightly positive (0.1–0.2 $V^{1/2}$). In any case, the intercept values calculated for a given pair of product ions should be approximately equal if our phenomenological explanation of this intercept arising through surface charging of the trapping plates is correct. In fact, the intercept calculated for the Ta^+ data is negative and significantly different from the intercept associated with the $C_6H_6^+$ produced during charge transfer with Ta^{2+}. Negative x intercepts have been observed in previous ICR measurements of kinetic energy release;[26] however, these were associated with reactions in which some fraction of the product ion population was born with little or no kinetic energy. Given the fact that our charge-transfer reactions produce two charged product ions, any resonable impact parameter for charge transfer must result in significant kinetic excitation of the product ions, if only due to the Coulombic repulsion of these products. Clearly, the negative x intercept in the Ta^+ data must arise in some alternative manner. Inspection of Figures 3–6 shows that, while there are a large number of data points available to fit the linearly increasing portion of the plot of Figures 3, 4, and 6, the heavy Ta^+ product is expected to carry away a relatively small kinetic energy and, therefore, only a small number of points lie on the linearly increasing portion of the plot in Figure 5 leading to significant uncertainty in the x intercept calculated for this plot. Given this uncertainty and in an effort to correct the Ta^+ data to the best of our ability, we have arbitrarily adjusted these data using the x intercept calculated for the $C_6H_6^+$ produced in this reaction.

Discussion

Conservation of linear momentum provides a simple test of the measured kinetic energy values. In the V^{2+}–benzene system, the kinetic energy determined for V^+, 0.99 ± 0.25 eV, indicates that the kinetic energy of $C_6H_6^+$ should be 0.65 ± 0.16 eV. While the agreement between this value and the measured kinetic energy, 0.92 ± 0.25 eV, is not ideal, there is significant overlap between the error limits of the two values, and the $C_6H_6^+$ kinetic energy is lower than that of V^+, as predicted. In the Ta^{2+}–benzene system, the Ta^+ kinetic energy, 0.90 ± 0.25 eV, suggests a $C_6H_6^+$ kinetic energy of 2.09 ± 0.58, in good agreement with the measured value of 1.92 ± 0.25 eV.

There are a number of interesting features of the data summarized in Table I. First, the kinetics studies show that each of these charge-transfer reactions proceeds with relatively high efficiency. Second, the kinetic energy plots in each case are well fit by a single kinetic energy value, suggesting that the reactions deposit relatively narrow distributions of energy into the various modes of the product ions. Gerlich has addressed the limitations of the ICR method for kinetic energy analysis,[36] and he suggests that breaks in the kinetic energy plots that occur at high values of $V_{eff}^{1/2}$ may be fit by a wide range of kinetic energy release distributions; however, our data were best fit by single values for the kinetic energy.

In our original study of Nb^{2+}–benzene charge-transfer dynamics, we addressed these observations by invoking a simple curve-crossing model to describe the charge-transfer event. The doubly charged ion and the neutral collision partner approach one another on an ion–induced dipole potential curve, $-\alpha q^2/2r^4$, where α is the polarizability of the neutral, q is the ionic charge, and r is the separation of the two species. The singly charged products of the charge-transfer reaction exit on a repulsive Coulombic potential, q^2/r. The energy difference between these two curves at infinite distance defines the critical distance at which these curves cross and electron transfer occurs.

This type of long-distance electron transfer might be expected to proceed in a "resonant" fashion. In the case of a reaction involving a singly charged ion and a neutral collision partner, reaction 4, resonant charge transfer requires that B^+ possess an

$$A^+ + B \rightarrow A + B^+ \quad (4)$$

excited electronic state with an energy relative to B that is nearly equal to the recombination energy of A^+. The resonance condition in the single charge-transfer reaction between a doubly charged ion and a neutral collision partner must also account for the Coulombic repulsion associated with the two singly charged product ions generated. So the reactions examined in this study could be said to proceed in a resonant fashion if in fact $C_6H_6^+$

(32) Chewter, L. A.; Sander, M.; Muller-Dethlefs, M.; Schlag, E. W. *J. Chem. Phys.* **1987**, *86*, 4737.
(33) Moore, C. E. In *Atomic Energy Levels as Derived from Analysis of Optical Spectra*; Office of Standard Reference Data; National Bureau of Standards: Washington, D.C., 1952; Vol. 2.
(34) Knott, T. F.; Riggin, M. *Can. J. Phys.* **1974**, *52*, 426.
(35) Sharp, T. E.; Eyler, J. R.; Li, E. *Int. J. Mass Spectrom. Ion Phys.* **1972**, *9*, 421.
(36) Gerlich, D. *J. Chem. Phys.* **1989**, *90*, 127.

TABLE II: Benzene Cation Electronic Energies and Orbital Assignments[a]

energy,[b] eV	orbital	energy,[b] eV	orbital
0.00	$1e_{1g}$	4.73	$3e_{1u}$
2.28	$3e_{2g}$	5.61	$1b_{2u}$
3.13	$1a_{2u}$	6.21	$2b_{1u}$

[a] See ref 6. [b] Each entry represents the difference between the experimental vertical ionization energies of the orbital in question and the $1e_{1g}$ orbital, $I_v - I_v(1e_{1g})$.

were produced in an excited electronic state with an energy relative to thermal neutral benzene equal to the second ionization potential of the group 5 transition metal in question less the kinetic energy partitioned to the ionic products.

The measured kinetic energies of the Nb^+ and $C_6H_6^+$ products in that system indicate that 3.05 ± 0.50 eV is deposited in the internal modes of these product ions during the charge-transfer event. In terms of the resonant long-distance charge-transfer model, this means that ~3 eV is deposited in the $C_6H_6^+$ product and relatively low internal energy Nb^+ is produced. Nb^+ supports a significant density of low-lying electronic states,[33] while there are considerably fewer low-lying electronic states of $C_6H_6^+$.[6] The orbital assignments and associated energies determined from the photoelectron spectrum of benzene are summarized in Table II. Of particular interest in this table is the $1a_{2u}$ orbital at 3.13 eV above the ground state of the benzene cation. By assuming that this charge-transfer reaction proceeds via a simple curve crossing at ~7.5 Å to ionize the $1a_{2u}$ orbital of benzene, the energy partitioning results can be explained in terms of a resonant long-distance electron transfer. This explanation is also appealing in that significant excitation of Nb^+ would probably lead to broad energy distributions given the dense manifold of states associated with this ion, while production of electronically excited $C_6H_6^+$ would lead to a narrower distribution of energies. The Franck–Condon envelope associated with this orbital shows significant intensity over an energy range from about 2.6 to 3.6 eV relative to the benzene cation ground state, and this range represents an upper limit to the width of the energy distributions in this reaction assuming this explanation of the energy partitioning is accurate.

The data for the V^{2+}–benzene system provide additional support for this simple model of the charge-transfer dynamics. The internal energy deposited in the product ions is 3.50 ± 0.50 eV, which is essentially the same as that observed in the Nb^{2+}–benzene system, given the error limits, and is also consistent with production of $C_6H_6^+$ in the excited electronic state arising from ionization of the $1a_{2u}$ orbital. The total kinetic energy released in the V^{2+}–benzene system implies a curve-crossing distance of ~7.9 Å (Figure 7), which is very close to the 7.5-Å value determined for Nb^{2+}–benzene. The uncertainty in the kinetic energy measurements permits curve crossing as close as 6.4 Å and as far away as 10 Å in this case. These distances make sense in terms of the efficiency of the reaction and are consistent with the long-distance electron-transfer model. So the results for the V^{2+}– and Nb^{2+}–benzene cases begin to suggest that the dynamics of the single-charge-transfer reactions of group 5 transition-metal dications with benzene are controlled by a resonance criterion satisfied through ionization of the $1a_{2u}$ orbital of benzene.

Our experimental measurements of the energy partitioning in the Ta^{2+}–benzene system raise a number of interesting questions and suggest a more complex picture. The first important observation is that while the charge-transfer reaction exothermicities in the V^{2+}–benzene (5.41 eV) and Nb^{2+}–benzene (5.08 eV) systems are approximately the same, the exothermicity in the Ta^{2+}–benzene case is significantly larger, 6.96 eV. Despite this difference, the internal energy of the Ta^+ and $C_6H_6^+$ products, 4.14 ± 0.50 eV, is not that different from that observed in the other two systems. In fact, considering the size of the error limits, the internal energy may be the same in each case, ~3.5 eV.

A second important aspect of the data for this system becomes evident when we recognize that the lowest energy dissociation process for $C_6H_6^+$, reaction 5, has an activation energy of ~3.8 eV.[37] Given that the $C_6H_6^+$ generated during the charge-transfer

$$C_6H_6^+ \rightarrow C_6H_5^+ + H^\bullet \quad (5)$$

reaction with Ta^{2+} is stored in the cell for up to 300 ms, it is reasonable to expect that process 5 would be observed if this ion were generated with ≳3.8-eV internal energy. In fact, no $C_6H_5^+$ was observed, placing an upper limit on the energy deposited in the $C_6H_6^+$ product during the course of the reaction. It is difficult to unambiguously interpret this aspect of the data in light of the large error limits on the internal energy of this system. At the low extreme of the error limits, the internal energy of the system is consistent with this limit, and all of this energy could conceivably be partitioned to the $C_6H_6^+$ product. In fact, the $1a_{2u}$ orbital of benzene exhibits nonnegligible intensity to ~3.75 eV above the ground state of the benzene cation, so the dynamics of the Ta^{2+}–benzene charge-transfer reaction are not in direct conflict with the simple resonant long-distance electron-transfer model. However, if the internal energy of this system is indeed on the order of ~4 eV, the absence of $C_6H_5^+$ in our experiment would indicate that the Ta^+ product is generated with some degree of electronic excitation.

The curve-crossing distance calculated by using the simple model based on the measured kinetic energy release in the Ta^{2+}–benzene system is ~5.7 Å (Figure 8) but may be as close as 5.0 Å and as far away as 6.7 Å, given the error limits on the kinetic energy measurements. Once again, the spread in the possible values complicates comparison with the other systems; however, the distance in this system is not significantly different from that of the other two group 5 systems.

A closer look at calculated curve-crossing distances for various degrees of $C_6H_6^+$ internal excitation is instructive. For example, given the simple model in which electronically excited $C_6H_6^+$ and an internally cold metal ion are formed, we have proposed that ionization of benzene occurs via the $1a_{2u}$ orbital. What if this ionization were to occur via the $3e_{1u}$ orbital, which lies 4.73 eV above the benzene cation ground state? This process would require the release of total kinetic energies of 0.68, 0.35, and 2.23 eV in the V^{2+}, Nb^{2+}, and Ta^{2+} cases, respectively. These kinetic energy releases correspond to curve-crossing distances of approximately 22, 41, and 6.9 Å; however, highly efficient charge-transfer reactions are expected to occur only when the species involved are sufficiently close to experience extensive electronic overlap. In fact, charge transfer is expected to proceed efficiently in the range 2–6 Å.[38] On the basis of the curve-crossings distances required for ionization of the $3e_{1u}$ orbital, it is highly unlikely that V^{2+} and Nb^{2+} will proceed via this pathway. The absence of $C_6H_5^+$ in each of these systems is evidence that benzene is not ionized via the $3e_{1u}$ orbital, and yet the curve-crossing distance for this process in the Ta^{2+}–benzene case is only ~6.9 Å, and it is not unreasonable to expect the charge-transfer reaction to proceed via this pathway. Clearly, this raises important questions about the validity of the simple model and suggests that more complex dynamics, especially involving excitation of the transition-metal product ion are likely to be involved.

Conclusions

Our studies of energy partitioning in the single charge-transfer reactions between M^{2+} (M = V, Nb, Ta) and benzene are consistent with a long-distance electron-transfer mechanism in which the dynamics are dictated by ionization of benzene via the $1a_{2u}$ orbital. The mechanism and the curve-crossing distances predicted by using a simple model on the basis of the observed kinetic energies also explain the high efficiencies observed in the reaction kinetics studies and the relatively narrow distributions of product energies observed.

While our measurements clearly demonstrate that product ions in these charge-transfer reactions possess significant kinetic energies, the semiquantitative values obtained limit our dynamical insight and the sophistication of our model of these reactions.

(37) Lias, S. G.; Bartmess, J. E.; Liebman, J. F.; Holmes, J. L.; Levin, R. D.; Mallard, W. G. *J. Phys. Chem. Ref. Data, Suppl. 1* **1989**, *6*.
(38) Smith, D.; Adams, N. G.; Alge, E.; Villinger, H.; Lindinger, W. *J. Phys.* **1980**, *B13*, 2787.

More complex dynamics in which electronically excited transition-metal product ions are generated in addition to excited $C_6H_6^+$ may be involved, and there is some evidence to suggest that this is the case.

However, in a straightforward picture of the charge-transfer event, the intense field associated with the doubly charged metal ion is responsible for pulling an electron from the benzene neutral. This process is quite similar to photoionization or field ionization of benzene, so it is not unreasonable to expect that the electronic structure of the nascent benzene ion will dictate the dynamics in these thermal charge-transfer reactions. An ideal experiment for interrogating the internal energy of the $C_6H_6^+$ product based on the sequential two-photon dissociation of the ion can be envisioned.[39] Fluence-dependence studies of the photodissociation of the excited $C_6H_6^+$ generated in these charge-transfer reactions performed at a number of critical photon energies would clearly establish the internal energy of the nascent product ion. Hopefully, the interesting questions raised in this study will stimulate further experimental and theoretical investigations of the chemistry of multiply charged transition-metal ions.

Acknowledgment. This work was supported by the National Science Foundation (CHE-8920085) and the Division of Chemical Sciences in the Department of Basic Energy Sciences in the United States Department of Energy (DE-FG02-87ER13766). J.R.G. gratefully acknowledges the National Science Foundation, the American Chemical Society and the Eastman Kodak Co. for fellowship support. We also acknowledge Extrel for the cell assembly currently installed in our FTMS-2000. In addition, we enjoyed helpful discussions with Dr. Denise Parent and Don Phelps and thank the referees for insightful comments.

Registry No. C_6H_6, 71-43-2; V^{2+}, 15121-26-3; Ta^{2+}, 35831-23-3.

(39) Freiser, B. S.; Beauchamp, J. L. *Chem. Phys. Lett.* **1975**, *35*, 35.

Optical Model Computations of Dissociative Chemisorption

David Farrelly*,† and R. D. Levine†,‡

Department of Chemistry and Biochemistry, University of California, Los Angeles, Los Angeles, California 90024, and The Fritz Haber Research Center for Molecular Dynamics, The Hebrew University, Jerusalem 91904, Israel *(Received: March 14, 1991)*

Activated dissociative chemisorption increases rapidly with the collision energy. For a given molecule and substrate, the dissociation probability can be quite different for different faces of the crystal. It is shown that the optical model can account qualitatively and quantitatively for these trends.

Introduction

In a seminar at UCLA in May 1990, R. B. Bernstein presented a grand overview of the recent work[1-6] of his group on the scattering of oriented molecules off graphite. In his talk and in discussions Professor Bernstein emphasized the wealth of systematic trends that were uncovered in this work. It seemed to him important that this data base serve not only as a reference for high-quality computational studies but also as a testing ground for models that could then be used to develop further understanding. Already during his visit to Jerusalem in May 1989 Professor Bernstein had started work on one such model, which he subsequently published with S. Ionov.[7] His long-time interest in intermolecular potentials and their systematics[8] made him also search for an understanding of the distinct steric preferences exhibited by different molecules as they approach a surface. The initial concept[2,4] that the relevant factor is the charge distribution in the molecule has recently[9] been refined in his work with D. A. Buckingham and others.

Since the early days of molecular reaction dynamics[12-17] the optical model[10,11] has been used to advantage in gas-phase collisions. In many ways the scattering of molecules off surfaces provides a most natural application of the model. The reason being the physical motivation provided by the optical potential model. In principle, whenever some products of a collision do not exit in the same channel as the reactants, one can introduce an optical model. As in the original application in optics, the physical interpretation is more obvious if the products are delayed (in time) with respect to the scattered reactants. The scattering theoretic model is thus most appropriate when it is possible to distinguish between a prompt scattering process and one that is delayed.[11,18]

Professor Bernstein repeatedly emphasized that a key experimental observation in his scattering experiments off graphite is the separation of the scattered signal into two identifiable components:[3,4] A directly scattered signal with a fairly narrow angular distribution and an essentially "cosine-law" distribution component. The latter was attributed to molecules that were trapped at the surface. Simulations[19] show that the component of the molecular momentum parallel to the surface may require a long time to be fully accommodated. Even so, in the experiments of Bernstein et al.[3,4] the resolution of the angular distribution into a direct and

†UCLA.
‡The Hebrew University.

(1) Curtiss, T. J.; Bernstein, R. B. *Chem. Phys. Lett.* **1990**, *168*, 45.
(2) Mackay, R. S.; Curtiss, T. J.; Bernstein, R. B. *Chem. Phys. Lett.* **1989**, *164*, 341.
(3) Mackay, R. S.; Curtiss, T. J.; Bernstein, R. B. *J. Chem. Phys.* **1990**, *92*, 801.
(4) Curtiss, T. J.; Mackay, R. S.; Bernstein, R. B. *J. Chem. Phys.* **1990**, *93*, 7387.
(5) Ionov, S. I.; LaVilla, M. E.; Mackay, R. S.; Bernstein, R. B. *J. Chem. Phys.* **1990**, *93*, 7406.
(6) Ionov, S. I.; La Villa, M. E.; Bernstein, R. B. *J. Chem. Phys.* **1990**, *93*, 7406.
(7) Ionov, S. I.; Bernstein, R. B. *J. Chem. Phys.*, in press.
(8) Bernstein, R. B.; Muckerman, J. T. *Adv. Chem. Phys.* **1967**, *12*, 389.
(9) Whitehouse, D. A.; Cho, V. A.; Bernstein, R. B.; Buckingham, D. A.; Levine, R. D., in this issue.
(10) Mott, N. F.; Massey, H. S. W. *The Theory of Atomic Collisions*; Clarendon Press: Oxford, 1965; Chapter VII.
(11) Levine, R. D. *Quantum Mechanics of Molecular Rate Processes*; Clarendon Press: Oxford, 1969; Chapter 3.4.
(12) Herschbach, D. R. *Adv. Chem. Phys.* **1966**, *10*, 319.
(13) Greene, E. F.; Moursund, A. L.; Ross, J. *Adv. Chem. Phys.* **1966**, *10*, 135.
(14) Roberts, R. E.; Ross, J. *J. Chem. Phys.* **1970**, *52*, 1464.
(15) Levine, R. D.; Bernstein, R. B. *Isr. J. Chem.* **1969**, *7*, 315.
(16) Rusinek, I.; Roberts, R. E. *Chem. Phys.* **1973**, *1*, 392.
(17) Micha, D. A. In *Dynamics of Molecular Collisions*; Miller, W. H., Ed.; Plenum Press: New York, 1976.
(18) Friedman, F. L.; Weisskopf, V. F. In *Niels Bohr and the Development of Physics*; Pergamon Press: Oxford, 1955.
(19) Head-Gordon, M.; Tully, J. C.; Rettner, C. T.; Mullins, C. B.; Auerbach, D. J. *IBM Res. Rep.* RJ 7721, 1990.

0022-3654/91/2095-8279$02.50/0